



Assessment of sub-surface water corrosion and encrustation potentials in parts of Eastern Dahomey Basin, Southwestern Nigeria

Richard Omotoso Fakolade 

Department of Mineral and Petroleum Resources Engineering Technology, The Federal Polytechnic, Ado Ekiti, Nigeria.

Abstract

Understanding hydro-geochemical parameters and corrosion-encrustation tendencies in coastal aquifers is crucial for sustainable water quality management. In the eastern Dahomey Basin of southwestern Nigeria, rapid deterioration of metal pipes, surface tanks, and boreholes has been observed, leading to significant infrastructure damage and failure. This study evaluates groundwater quality and assesses corrosion and encrustation potentials using multiple geochemical indices. Twenty groundwater samples were collected and analyzed for physicochemical parameters (pH, Electrical Conductivity (EC), Temperature (°C), Total Dissolved Solids (TDS)) and chemical constituents including hardness, chloride, manganese, and iron using Atomic Absorption Spectrophotometry (AAS) and titration. Physicochemical and ions concentration analysis results were further adopted to compute corrosion and encrustation indices including; Langlier Index (LSI), Ryznar Stability Index (RSI), Larson-Skold Index (LS), and Aggressive Index (AI) were computed. Results indicate LSI values of the samples were corrosive while they exhibited higher scaling tendency. AI indicated moderately corrosive and scaling-prone; RSI results ranging from high corrosive to severely corrosive nature; LS indicated high concentration scaling-prone with mild corrosive status. Spatial analysis revealed higher corrosion tendencies near coastal zones due to seawater intrusion influences. The study highlights the need for corrosion-resistant materials and preventive measures in groundwater infrastructure development.

Article Information

Publication type: Research Papers
Received 27 July 2025
Accepted 16 January 2026
Online pub. 2 February 2026
Editor: Joana A. G. da Luz

Keywords:
Aggressive Index
Hydro-geochemical
Total Dissolved Solids
Coastal aquifers
Seawater intrusion

*Corresponding author
Richard Omotoso Fakolade
E-mail address: fakolade_ro@fedpolyado.edu.ng

Accepted manuscript – Uncorrected pre-proof

This is a PDF file containing an unedited and non-definitive version of a manuscript that has been accepted for publication by the **Journal of the Geological Survey of Brazil – JGSB**, which serves to provide early visibility of the article. Being an uncorrected pre-proof version, errors may appear during the production process (language review, formatting and proof review), and these can affect the final content of the article and all legal disclaimers (<https://jgsb.sgb.gov.br/index.php/journal/6>).



This work is licensed under a Creative Commons Attribution 4.0 International License.

ISSN: 2595-1939

<https://doi.org/10.29396/jgsb.2026.v9.n1.5>

Open access at <https://jgsb.sgb.gov.br>

1. Introduction

Hydrochemical evaluation of groundwater is essential for understanding geochemical processes, rock-water interactions, and anthropogenic influences on water quality (Olofinlade et al., 2018). The hydrochemical behavior of groundwater and its tendency to corrode or encrust well infrastructure is explained by theories of water–rock interaction, electrochemical corrosion, and carbonate scaling. The Langelier, Ryznar, and Larson–Skold indices, alongside WHO and Johnson guidelines, provide predictive frameworks for assessing water aggressiveness. The Langelier Saturation Index (LSI) is one of the most commonly used indices for assessing carbonate equilibrium in groundwater. It is defined as the difference between the measured pH and the saturation pH of calcium carbonate.

Negative LSI values indicate under saturation and corrosive conditions, where groundwater has the potential to dissolve protective CaCO_3 films, while positive values suggest supersaturation and a tendency toward carbonate scaling (Langelier, 1936; Stumm & Morgan, 1996). Although LSI is effective in identifying scaling conditions, it may underestimate corrosion potential in waters influenced by elevated chloride or sulfate concentrations. To address this limitation, the Ryznar Stability Index (RSI) was developed as a refinement of the Langelier concept. RSI places greater emphasis on the stability of existing calcium carbonate films rather than saturation state alone. RSI values greater than 7 generally indicate corrosive water capable of dissolving protective scales, whereas values below 6 suggest scale-forming tendencies (Ryznar, 1944). Several studies have demonstrated that RSI correlates more closely with observed corrosion damage in groundwater systems than LSI, particularly in sedimentary and coastal aquifers (Roberge, 2007; Amah et al., 2008). To complement this.

The Larson–Skold Index (LS) was developed specifically evaluates the influence of aggressive anions by comparing the combined concentration of chloride and sulfate ions to bicarbonate alkalinity. This index is particularly relevant in coastal environments affected by saline intrusion, where elevated chloride levels promote localized pitting and tuberculation in iron and steel infrastructure. LS values greater than 1.2 indicate high corrosion risk, even in waters that may be classified as non-aggressive based on carbonate saturation indices alone (Larson & Skold, 1958; Trethewey & Chamberlain, 1995). The Puckorius Scaling Index (PSI) further refines scaling predictions by incorporating buffering capacity and equilibrium pH conditions. Unlike LSI, which represents an instantaneous saturation state, PSI accounts for the ability of groundwater to maintain or disrupt carbonate equilibrium over time. This makes PSI particularly suitable for groundwater systems subjected to seasonal recharge, variable abstraction, and fluctuating alkalinity, conditions commonly observed in shallow unconfined aquifers (Puckorius & Brooke, 1991).

In coastal aquifers, groundwater chemistry is influenced by complex interactions including seawater intrusion, mineral dissolution, and climatic variations (Aladejana et al., 2020). Corrosion and encrustation in water systems result from electrochemical reactions between metals and dissolved ions (Garg, 2005). Encrustation, caused primarily by mineral precipitation (CaCO_3 , Fe/Mn oxides), reduces borehole efficiency and flow capacity. Corrosion, accelerated by dissolved oxygen, chloride, and low pH, deteriorates metallic

infrastructure and compromises water quality (Omaka et al., 2014). Recent studies in coastal environments have demonstrated that seawater intrusion significantly exacerbates corrosion processes through increased ionic strength and chloride concentrations. Several researchers (Roberge, 2007; Amah et al., 2008; McGarvey, et al., 2008) have adopted Corrosion-Encrustation Index Parameters (CEIP) to investigate these processes in water systems, they reported that these metrics serve as reliable indicators for evaluating corrosion and encrustation levels in wells and pipeline systems (Winston, 2020). During post deposition and diagenesis of particles, corrosion continues, which may include multiple stages with total duration of tens to hundreds of millions of years (Turner and Morton, 2007). The Eastern Dahomey Basin represents one of the most important groundwater provinces in southwestern Nigeria, extending across Lagos, Ogun, and Ondo States (Figure 1). Its aquifer systems primarily composed of coastal plain sands, the Benin Formation, and Paleogene–Neogene deposits. These provide potable water to millions of residents in rapidly urbanizing areas where municipal surface-water infrastructure remains inadequate. Consequently, several boreholes and hand-dug wells were tapping these aquifers as their dominant sources of domestic, industrial, and agricultural water supply (Oyeyemi et al., 2023; Aladejana et al., 2021). Despite extensive research globally, the impact of these processes on groundwater infrastructure in the Eastern Dahomey Basin remains understudied. Recent hydrogeophysical investigations in the basin have identified two main aquifer systems with varying hydraulic parameters, highlighting the complex

Figure 1: Map of the study area showing sample locations (retrieved from Google)

hydrogeological setting that influences water chemistry. Additionally, elemental geochemistry studies of Cretaceous deposits in the basin have provided insights into paleo-environmental conditions that continue to affect contemporary water-rock interactions. This study aims to investigate groundwater quality in the Ilaje community and its environs within Ondo State, evaluate corrosion-encrustation potentials using multiple geochemical indices, and recommend mitigation strategies for sustainable water resource management in this coastal region.

2. Geology of the study area

The Dahomey Basin is a Cretaceous-Tertiary sedimentary basin extending along the southwestern coast of Nigeria. It is a marginal pull apart basin (Kingston et al., 2005), which advanced through the rifting era in the Late Jurassic to Early Cretaceous periods. This resulted from tectonic activities that were brought about by an extended period of thermally tempted basin subsidence from the Middle-Upper Cretaceous to Tertiary stretches as the South American and African tectonic plates entered a drift phase to accommodate the emerging Atlantic Ocean (Ikhane et al., 2018). The basin is bounded by the Ghana Ridge in the western section, while her eastern boundary is limited by the Benin hinge line, which splits Okitipupa subsurface ridges from the Niger Delta Basin (Olabode, 2015).. The eustatic sea-level fluctuation contributed to occurrence of normal faulted graben and horst

structure of the basin floor resulting to thick accumulations of sediments within the grabens (Madukwe et al., 2015). The basin comprises Cretaceous units of the Abeokuta Group (Ise, Afowo, and Araromi Formations) and Tertiary units (Figure 2, Table 1), including the Ewekoro, Akinbo, Oshosun, Ilaro, and Benin Formations (Fakolade and Obasi, 2012). The study area lies within the Coastal Plain Sands (Benin Formation) and Quaternary Alluvium, characterized by unconfined aquifers in sandy and clayey layers with varying hydraulic conductivity (Offodile, 2002; Olabode & Mohammed, 2016).

Figure 2: Geological map of the study area (Adapted from Olabode and Mohammed, 2016)

Table 1: Generalized stratigraphic column showing age, lithology, and aquifer characteristics in the eastern Dahomey Basin

The eastern sector of the Dahomey Basin has experienced complex depositional environments and diagenetic processes that influence contemporary hydro-geochemical conditions. Recent elemental geochemistry studies of the deposits within the basin have revealed predominantly oxic conditions with minor occurrences of suboxic environments, which affect the mobilization and precipitation of metals relevant to corrosion and encrustation processes. The aquifer units comprise unconfined and confined sand, sandstones, clayey sand, and dissolved/fractured limestone. Modal classification shows that sediments are primarily composed of quartz grains (70–80%) with other minerals making up the remaining 20%. Other mineral resources available in the area include glass sand, salt, tar sand, quartz, and clay (Figure 3).

The Ilaje Local Government Area (LGA) of Ondo State, southwestern Nigeria, occupies a long stretch of the eastern Dahomey Basin coastline. According to the 2006 national census, Ilaje had a population of 289,838 people, while more recent demographic projections suggest the population has grown to over 445,000 by 2022, reflecting steady national growth rates in coastal communities (National Population Commission, 2006; Akinyemi, et al. 2023). The climate of the area is characteristically tropical wet, classified under the Köppen system as rainforest/monsoon type (Af-Am). It is marked by consistently high humidity, uniformly warm temperatures, and a long rainy season extending from March/April to October/November. Mean annual rainfall values range from ~1,880 to over 2,340 mm, with September usually the wettest month (Ajibola and Adeoye, 2018; NiMet, 2018). Physiographically, the terrain is extremely low-lying, with digital elevation model (DEM) analyses indicating altitudes between -6.5 m and +4.5 m above mean sea level across much of the coastal plain, and slightly higher elevations of 12–29 m further inland. This morphology renders the area highly vulnerable to flooding, storm surge, and seawater intrusion (Fakolade et al., 2024).

The dominant soils are Arenosols, Gleysols, and Acrisols, reflecting sandy barrier deposits, swamp/alluvial environments, and weathered tropical soils, respectively (Figure 4). Extensive estuaries, lagoons, and mangrove wetlands further characterize the geomorphology of Ilaje (Adegun and Olowolafe, 2018). Socio-economically, Ilaje is primarily a fishing community, with artisanal fisheries, fish processing, and canoe building forming the major livelihoods (Oladimeji and Adubi, 2020). Coconut plantations and smallholder farming are practiced in less waterlogged zones, while parts of the LGA overlap with

Nigeria's petroleum-producing coastal belt, adding oil and gas activities to the economic profile but also heightening environmental pressures (Adeyemi and Olayinka, 2019).

Figure 3: Photographs of outcrops from the study area showing sedimentary sequences

Figure 4: Map of the study area showing sampling point locations

3. Materials and methods

3.1 Sample Collection and analysis

Twenty (20) groundwater samples from boreholes and wells at different locations within the study area (Figure 4) were collected in sterile 2-liter plastic bottles that had been pre-cleaned with nitric acid and rinsed with deionized water. The spatial selection of groundwater sampling locations was designed to ensure adequate representation of the hydrogeochemical variability across the study area while capturing gradients in lithology, land use, and proximity to potential salinity and contamination sources. Sampling points were distributed to achieve broad spatial coverage, minimize clustering bias, and allow reliable spatial interpolation of hydrochemical indices using geostatistical techniques. Sampling locations were selected based on; hydrogeological setting, including variations in aquifer lithology and depth; spatial distribution, ensuring uniform coverage across inland and coastal zones; and anthropogenic influence, such as proximity to settlements, agricultural activities, and water abstraction points. This approach is consistent with established groundwater sampling protocols, which recommend stratified spatial sampling to capture both natural geochemical evolution and localized perturbations arising from human activities (Freeze and Cherry, 1998; Appelo and Postma, 2005).

Each sample was stored in ice-cooled containers at 4°C and transported to the laboratory for analysis within 24 hours of collection. In-situ measurements of pH, electrical conductivity (EC), temperature, dissolved oxygen, and bicarbonate were conducted using calibrated portable meters (Hanna Instruments HI98194 multiparameter meter for pH/EC/DO, and Hach digital titrator for alkalinity). For the laboratory chemical parameters measurements, a 250 ml conical flask was filled with 100 ml of samples that had been acidified with 5 ml of conc. HNO_3 , and then 5 ml of conc. HCL was added. The flask was then heated on a hot plate to roughly 600°C for 15 minutes. After being taken out of the oven, the flask was cooled in desiccator and filtered. A standard volumetric flask was used to collect the filtrate from the flask, and an Atomic Absorption Spectrometer (AAS; PerkinElmer PinAAcle 900T) was used to analyze for Fe, Ca, Mg, and Mn and anions (Cl^- , SO_4^{2-} , NO_3^- , HCO_3^-) using ion chromatography (Dionex ICS-1100) and titration methods where appropriate. Total dissolved solids (TDS) were calculated from EC measurements using a conversion factor of 0.67. Quality assurance and control measures included analysis of certified reference materials (CRM), duplicate samples, and blank samples. Ionic balance errors were calculated and maintained within $\pm 5\%$ for all samples, confirming the reliability of the analytical data. Determining the carbonate scale in groundwater, additional calculations were made using the Ryznar stability and other indices (Ryznar 1944) were computed.

3.2 Corrosion and Encrustation Indices

The corrosion and encrustation potential of groundwater samples was evaluated using the following indices:

1. Langelier Saturation Index (LSI): $LSI = pH - pHs$ (1)
where pHs is the pH at which water is saturated with $CaCO_3$.
2. Ryznar Stability Index (RSI): $RSI = 2pHs - pH$ (2)
3. Larson-Skold Index (LS): $LS = [Cl^- + SO_4^{2-}] / [HCO_3^- + CO_3^{2-}]$ (3)
4. Aggressive Index (AI): $AI = pH + \log[(Alk) (Hardness)]$ (4)

Where all ionic concentrations are expressed in mg/L. The classification criteria for these indices are summarized in Tables 2 and 3.

Table 2: Corrosion -Encrustation Indices equations and their interpretations

Table 3: Classification criteria for corrosion and encrustation indices

This sophisticated equation was created to improve the Langelier (1936) equation. According to the equation, water will dissolve $CaCO_3$ scale when the Ryznar index value is less than six (6), whereas values more than six (6) indicate the likelihood of the water forming $CaCO_3$ scale. As a control check to ensure the accuracy of the analyzed data, ions were translated from milligram per litre to milli-equivalent per litre, and anions were balanced against cations. The Corrosion and Encrustation Indices were computed using standard formulas (Tables 2 and 3).

3.3 Spatial Analysis and statistical methods

Geospatial analysis was conducted using interpolated contour map plotted from sigma plot software for distribution of corrosion and encrustation potentials across the study area. Statistical analysis including correlation matrices was performed using SPSS version 26 to identify relationships between hydrochemical parameters and corrosion indices.

4. Results

4.1 Hydrochemical characteristics

Based on the analysis conducted on the samples under study, physicochemical analysis results revealed pH values ranging from 6.3 to 7.5 (mean 7.0), indicating mildly acidic to neutral conditions (Tables 2 and 3). TDS concentrations varied from 378 to 1078 mg/L (mean 684.8 mg/L), while Electrical conductivity ranged from 714 to 2037 μ S/cm (mean 1424.7 μ S/cm). Water temperatures ranged from 25°C to 30°C (mean 27.5°C). Salinity, expressed in practical salinity units (PSU), ranged from 0.03 to 0.9 (mean 0.4) as presented in Tables 4 and 5.

Table 4: Results of Physicochemical analysis from the study area

Table 5: Statistical summary of physicochemical parameters of groundwater samples in relation to WHO (2017) standards.

Chemical analysis showed bicarbonate levels ranging from 180 to 600 mg/L (mean 350 mg/L), chloride from 7.1 to 47.9 mg/L (mean 17.2 mg/L), sulfate from 2.1 to 4.9 mg/L

(mean 3.5 mg/L), and nitrate from 0.02 to 12.3 mg/L (mean 7.4 mg/L). Major cations include sodium (0.1-24 mg/L, mean 1.2 mg/L), calcium (21.0-79.9 mg/L, mean 45.8 mg/L), and magnesium (82.1-318.1 mg/L, mean 197.6 mg/L). Iron concentrations ranged from 0.3 to 0.8 mg/L (mean 0.5 mg/L) (Tables 6 and 7).

Table 6: Results of Ion Concentrations analysis of the samples under study.

Table 7: Statistical summary of Ion Concentrations parameters of groundwater samples.

4.1.1 Corrosion and Encrustation Indices

Calculation of corrosion and encrustation indices revealed varied tendencies across the study area (Tables 8 and 9). The Langelier Saturation Index (LSI) showed 41% of samples were corrosive ($LI < 0$), while 59% exhibited scaling tendency ($LI > 0$). The Ryznar Stability Index (RSI) indicated 88% of samples were corrosive ($RSI > 6$) and 12% were severely corrosive ($RSI > 8$). The Aggressive Index (AI) showed 41% of samples as moderately corrosive ($AI < 10$) and 59% as scaling-prone ($AI > 12$). The Larson-Skold Index (LS) indicated 62% of samples as scaling-prone ($LS < 0.8$) and 38% as corrosive ($LS > 1.2$).

Table 8: Stability Indices Results per Sample from the study area

Table 9: Summary of Corrosion and Encrustation indices for groundwater samples under study

5. Discussion

5.1 Hydrochemical controls on corrosion and encrustation

The groundwater chemistry of the eastern Dahomey Basin reveals complex interactions between natural geochemical processes and anthropogenic influences that affect corrosion and encrustation potentials. The pH values (6.3 - 7.5) indicate mildly acidic to neutral conditions, with approximately 41% of samples showing $pH < 7.0$. Lower pH enhances corrosion through proton-induced metal dissolution and destabilization of protective scales. The remaining 59% of samples with $pH > 7.0$ favor carbonate precipitation leading to encrustation, consistent with findings in similar coastal aquifers (Offodile, 2002). Electrical conductivity values showed that four samples (T2, T5, T6, and T7) exceeded the WHO (2017) permissible limit of 1500 μ S/cm, indicating higher ionic strength that can accelerate corrosion processes. The correlation between EC and chloride concentration ($R^2 = 0.72$) suggests seawater intrusion as a contributing factor to elevated conductivity in coastal samples. This is particularly evident in samples collected within 5 km of the coastline, which showed 40% higher corrosion indices than inland samples.

The elevated magnesium concentrations (82.1 - 318.1 mg/L) in all samples significantly exceed the WHO (2006) permissible limit of 50 mg/L, contributing to increased water hardness and potential scaling tendencies. Magnesium ions can participate in corrosion processes through competitive adsorption and can form protective layers that reduce corrosion rates but contribute to scale formation. Iron concentrations (0.3-0.8 mg/L) exceeded WHO limits in 70% of samples,

indicating significant potential for iron-related encrustation through oxidation and precipitation of ferric hydroxides. The presence of iron bacteria in such environments can accelerate these processes through biological oxidation.

The sulfate concentration (SO_4^{2-}) in the study area's groundwater falls below the allowable threshold level. Despite this, sulfate ions present might have influenced water's corrosivity in this study by contribute to mineral deposits when interacting with other elements. The slight acidity of groundwater, possibly exacerbated by acid rain, may increase sulfate levels over time, impacting corrosion processes (Johnson, 1975; Obiefuna and Orazu like, 2011). The chloride-sulfate ratio ($\text{Cl}^-/\text{SO}_4^{2-}$) exceeded 4 in 65% of samples, suggesting potential sulfate-reducing bacterial activity that can produce corrosive hydrogen sulfide. This is particularly concerning in confined aquifer systems where anaerobic conditions prevail, and capable of producing corrosive H_2S (Laniyan et al., 2024). The nitrate concentration (NO_3^-) measured values are well below the WHO (2006) maximum tolerable limit of 50 mg/l. This suggests a low risk of nitrate-related health concerns, such as methemoglobinemia or carcinogenic effects. Phosphate (PO_4^{3-}) levels in this study is low, although there is no specified WHO standard for phosphate in drinking water, but high phosphate concentrations can promote algal blooms and eutrophication in near surface and groundwater systems. The concentration of (NO_3^-) measured in this study suggest an environment with low microbial or biological activity that would otherwise be stimulated by phosphates.

Sodium (Na^+) concentrations in the water samples under study revealed values that are significantly below the WHO permissible limit of 250 mg/l, indicating no adverse effects related to sodium levels. The low sodium content suggests minimal impact on water taste or health concerns related to sodium intake. Calcium (Ca^{2+}) generally contributes to water hardness and stability of pH, which can influence corrosion and scaling (Figure 5). The absence of an explicit WHO acceptable standard implies these levels are within ranges for drinking water. The Magnesium (Mg^{2+}) concentrations of the samples under study exceed the WHO (2006) permissible limit of 20 mg/l, indicating high levels of hardness. Excess magnesium contributes to increased water hardness, which can lead to scaling and potential operational issues in plumbing and industrial processes.

Figure 5: Spatial distribution based in IDW Interpolation of (A) pH (B) electrical conductivity/TDS physicochemical parameters, and ion concentrations maps including (C) chloride, and (D) calcium across the study area

The iron (Fe^{3+}) concentration in the water samples revealed about 70% is above the WHO (2006) permissible limit of 0.3 mg/l, while the remaining 30% fall below the permissible limit. This indicates that iron levels have higher impact on the water quality. Iron in water exists in soluble ferrous (Fe^{2+}) and insoluble ferric (Fe^{3+}) forms. When dissolved, iron makes water clear and colorless; however, upon exposure to air, it oxidizes to ferric form, resulting in reddish-brown sediments. Given the high iron concentration, its influences on corrosion or scaling in the study area are considered significant.

The TDS of the samples under study reflect areas with warmer colours indicate more mineralised water. The high values around T6, T12, T16 and T18 suggest mineralised

groundwater, probably from long residence time or water and rock interaction. High TDS greater than (1000 mg/L) will cause the water to be more mineralized, often with higher chloride, sulfate, and bicarbonate. Therefore, elevated TDS increases electrical conductivity, allowing galvanic or chemical reactions with metals pipes, pumps and well screens. This contributed to the occurrence of corrosive nature of these materials. On the other way, high TDS usually means more dissolved Ca^{2+} , Mg^{2+} , and HCO_3^- , which can precipitate as CaCO_3 or MgCO_3 when pressure or temperature changes leading to encrustation on the metallic materials as well (Tables 10 and 11).

Higher salinity zone is observed in sediment sample T13 with about 3‰, this indicates significant isolation of dissolved salts (chlorides/sulfates) in this area. Most of these samples revealed fresh salinity (< 1‰), except sample T13, which may reflect localised contamination, evaporation, or mixing with more saline groundwater. Salty water is aggressive toward steel and concrete because Cl^- and SO_4^{2-} accelerate pitting and rust (Barlow, 2003). At the same time, if bicarbonate and hardness are also high, calcium carbonate scale may form, this will partially protect the pipes but clogging screens

Moderate Bicarbonate (HCO_3^-) ranging between (200–620 mg/L is observed in this study area, this signify an enhanced alkalinity and buffering capacity. Where pH is neutral to slightly alkaline (6.8–7.5), bicarbonate can combine with $\text{Ca}^{2+}/\text{Mg}^{2+}$ to form carbonate scales, leading to encrustation in wells, filters, and pipelines. Whereas, at a very low pH, HCO_3^- may convert to carbonic acid resulting to mildly corrosive (Tables 10 and 11).

Table 10: Description of corrosion and encrustation indices compared with various standards

Table 11: Descriptive summary of corrosion and encrustation indices reference to specific sample locations.

5.2 Hydrochemical facies

A Piper diagram was plotted using Piper and Durov plots system (Figure 6), this classifies water based on the relative abundance of major cations (Ca^{2+} , Mg^{2+} , Na^+/K^+) and anions (HCO_3^- , SO_4^{2-} , Cl^-). Although we don't yet have a full suite of cations/anions, the data on HCO_3^- , TDS, pH and salinity suggest: Waters with high HCO_3^- and moderate TDS (T3, T4 and T14) are likely $\text{Ca}-\text{Mg}-\text{HCO}_3$ facies, typical of fresh groundwater recharging through carbonate-bearing rocks. Sites with elevated TDS/salinity (T6, T12, T16 and T18) indicate evolution toward a mixed $\text{Ca}-\text{Na}-\text{HCO}_3/\text{Cl}$ type, implying longer residence or partial mixing with deeper mineralised water. T13, with salinity $\approx 3\text{‰}$, likely belongs to a NaCl facies, characteristic of brackish water or contamination (Appelo & Postma, 2005). By implication, $\text{Ca}-\text{Mg}-\text{HCO}_3$ facies are prone to carbonate scaling ($\text{CaCO}_3/\text{MgCO}_3$), whereas NaCl waters signify more corrosive because Cl^- promotes pitting and dissolves protective films (Figure 6).

Figure 6: Piper diagram plotted using the Piper trilinear plot indicating hydrochemical facies of the samples under study

5.2.1 Corrosion and Encrustation Potentials

Analysis of the parameters such as pH, Ryznar Scaling Index (RSI), Larson-Skold Index (LS), Puckorius Scaling Index (PSI), Aggressive Index (AI), and Langlier Saturation

Index (LSI) (Table 5) indicates that the overall corrosion and encrustation potential in the groundwater under study are approximately round 30%, with the remaining 40% showing neutral characteristics. Spatial variations suggest that different aquifers have differing tendencies for salt-induced encrustation or corrosion, but on average, these effects are moderate across the study area.

Langelier Saturation Index (LSI) indicates about 41% of the samples under study fall between -0.6 and -0.3, this confirms under-saturation conditions with respect to CaCO_3 . This signifies the aggressive nature of the water capable of dissolving protective scales (Stumm & Morgan, 1996). It is also observed 59% of samples signify positive LSI (0.1-1.2), this suggests scaling potential, with highest values of TDS in samples T6 and T12.

LSI strengths on samples under study. In this study LSI directly addresses carbonate scale versus under saturation, this indicates it is useful where Ca^{2+} and HCO_3^- are major controls on protective carbonate films (common among the shallow aquifers). It is simple to compute from routine lab measurements (pH, alkalinity, calcium, TDS/temperature),

Some limitations: some of the under study samples where carbonate interaction dominates corrosion/scaling, it is observed seawater intrusion raises Na^+/Cl^- and sulfate, thereby increases ionic strength. This allows corrosion mechanisms to shift from carbonate-film control to chloride-induced pitting and general ionic-strength-driven corrosion resulted to corrosivity underestimation. Also, high salinity from seawater intrusion increases ionic strength and makes activity corrections important. LSI doesn't capture non-carbonate aggressors (dissolved oxygen, CO_2 partial pressure changes, chloride pitting), that are known drivers in coastal aquifers.

The Ryznar Stability Index (RSI) addresses the corrosion risk of soil samples. It was observed that 88% of samples have values $\text{RSI} > 7$ indicating severe corrosion risk, particularly in T3 and T15 where chloride exceeds 30 mg/L. The strong correlation ($R^2=0.76$) between RSI and chloride concentration supports the chloride-induced corrosion mechanism described by Roberge (2007).

Strengths. Based on this study, RSI often correlates better with observed corrosivity in distribution systems for waters that are undersaturated with respect to CaCO_3 hence the useful in preliminary screening of groundwater that may attack metal infrastructure. Also, it is simple to compute from the same field/lab data (pH, alkalinity, Ca^{2+} , T), and good for rapid assessments in large sample sets.

Limitations: RSI's calibration and thresholds were developed historically for certain temperate waters and may not translate directly where chloride-driven corrosion dominates, but relevant where seawater mixing, evaporites, and organic inputs occur. In shallow coastal aquifers where CO_2 degassing, pressure changes and temperature vary. RSI can be misrepresenting unless field protocols are tight.

Aggressiveness index of the groundwater samples under study range from 6.345 to 9.317 with a mean value of 8.045. This indicates the sample has 100% corrosion potential, 0% encrustation potential, and 0% neutral potential. As a result of the high concentration of degrading components in the water, the finding suggests that the borehole pipes and well of the research region are likely to be corrosive and hazardous to human health (Figure 7).

Strengths: AI uses pH, alkalinity and hardness parameters often available from routine sampling, making it attractive for rapid screening across many wells in the basin. AI can approximate the protective effect of CaCO_3 film without detailed equilibrium calculations and handy when lab resources are limited.

Figure 7: Spatial distribution of (A) Langelier Saturation Index (LSI), (B) Aggressive index, (C) Ryznar Stability Index (RSI) and (D) Larson-Skold Index values across the study area. The IDW approach applies a distance-decay weighting, ensuring that nearby water samples exert greater influence on interpolated values, which aligns with the localized nature of groundwater quality variation in the study area.

Limitations: Inconsistency in calculation methods can produce different classifications unless a single standard method is used. Insensitive to chloride/sulfate-driven pitting and to redox/biological factors, both relevant in coastal aquifers. AI can therefore miss major drivers of infrastructure corrosion in eastern Dahomey Basin coastal zones.

The Larson-Skold Index (LS) revealed 38% of samples under study to be greater than 1.2; this indicates a high chloride-sulfate corrosion, particularly in wells less than 30m depth. The remaining 62% with $\text{LS} < 0.8$ show stable Fe(OH)_3 films, consistent with observations by Larson and Skold (1958) in iron-rich aquifers.

Strengths: It is directly sensitive to halide (Cl^-) and sulfate loading; this is a major advantage in coastal aquifers in eastern Dahomey Basin where seawater intrusion elevates Cl^- and SO_4^{2-} . LS can therefore pick up chloride-driven aggressiveness that carbonate-based indices miss. Multiple Dahomey Basin studies report elevated chloride/TDS near the coast, making LS highly relevant. This Predicts localized pitting and acid-type attack risk better than LSI in waters with high halide content (seawater-impacted).

Limitations: The Larson-Skold empirical relationships were calibrated on Great Lakes waters and steel pipes; extrapolation to other materials (concrete, copper, modern alloys) or to eastern Dahomey Basin's specific conditions requires caution. This doesn't include pH, DO, temperature in its action. These factors strongly affect corrosion rates. LS alone may fail to predict actual field corrosion without those data.

5.2.2 Spatial Distribution of Corrosion and Encrustation Potentials

Spatial analysis revealed clear patterns in corrosion and encrustation potentials across the study area (Figure 7). Samples from coastal locations (within 5 km of coastline) showed significantly higher corrosion tendencies, attributed to seawater intrusion increasing ionic strength and chloride concentrations. The influence of tidal pumping on oxygen diffusion and mixing processes further enhances corrosion in these zones. Agricultural areas showed elevated nitrate concentrations (up to 12.3 mg/L) that can promote microbial corrosion through nutrient availability for corrosion-related bacteria. Industrial zones exhibited higher sulfate concentrations (up to 4.9 mg/L) and lower pH values (as low as 6.3), accelerating electrochemical corrosion processes (Revie and Uhlig, 2008).

The spatial distribution of LSI values shows scaling tendencies predominant in inland areas where carbonate mineral dissolution increases calcium and bicarbonate

concentrations, while corrosive tendencies dominate in coastal areas influenced by seawater intrusion (Figure 7).

Spatial interpolation of Corrosion and Encrustation Indices using Inverse Distance Weighting (IDW): In this study, Inverse Distance Weighting (IDW) was chosen for spatial interpolation of corrosion and encrustation indices (LSI, AI, LS) across the Eastern Dahomey Basin sampling points. IDW was preferred because the dataset consisted of 20 moderately clustered samples, insufficient for reliable variogram modeling required by geostatistical Kriging. Furthermore, corrosion indices are locally sensitive hydrochemical parameters, for which deterministic methods such as IDW provide more robust and interpretable spatial patterns.

5.3. Global Perspectives on Corrosion and Encrustation Studies

The hydrochemical behavior observed in this study shows strong consistency with earlier regional investigations while also highlighting important local variations. The classification of approximately 30% encrustation potential aligns closely with findings from the Niger Delta aquifer systems, where Amah et al. (2008) reported moderate to high encrustation tendencies largely controlled by iron-rich groundwater, reducing conditions, and microbial activity. In both cases, iron precipitation—rather than carbonate scaling—plays a dominant role, reflecting similar sedimentary environments, organic matter abundance, and redox-sensitive geochemical processes typical of deltaic settings (Revie and Uhlig, 2008). However, the corrosion potential identified in this study exceeds values reported for the Benin Formation by Offodile (2002). This discrepancy is plausibly attributed to elevated chloride concentrations, which significantly enhance water aggressiveness by increasing electrical conductivity and promoting electrochemical reactions on metal surfaces. Chloride-induced corrosion has been widely documented in coastal and near-coastal aquifers worldwide, where marine influence, saline intrusion, or evaporative concentration intensifies corrosive conditions compared to inland sedimentary basins.

Furthermore, the mechanism of encrustation in the present study differs fundamentally from carbonate-dominated systems described in northern Nigeria. Etu-Efeotor (1997) demonstrated that groundwater scaling in crystalline and semi-arid northern terrains is largely driven by calcium carbonate precipitation, controlled by high alkalinity, elevated pH, and temperature-induced degassing of CO_2 . In contrast, the current study area exhibits iron-dominated encrustation, governed by redox fluctuations, iron oxidation, and microbial mediation rather than carbonate equilibrium. Similar iron-controlled scaling processes have also been reported in deltaic and alluvial aquifers in parts of Asia and South America, emphasizing the strong influence of depositional environment and groundwater chemistry on scaling mechanisms. Overall, these comparisons underscore that while the encrustation and corrosion indices observed in this study are regionally consistent with other Nigerian and global sedimentary aquifers, local geochemical conditions particularly chloride levels, redox state, and dominant mineral phases—play a decisive role in determining the severity and type of infrastructure deterioration in groundwater systems. Recent studies on coastal aquifer management have

highlighted the increasing threat of seawater intrusion due to climate change and sea-level rise, which exacerbates corrosion problems in coastal infrastructure (Abd-Elaty, et al., 2022). The findings of this study align with global observations that coastal groundwater systems are experiencing increasing corrosion risks due to changing hydrological conditions (Oyeyemi et al., 2023).

The iron encrustation mechanism differs from carbonate-dominated systems in northern Nigeria, reflecting the unique hydrogeochemical environment of the coastal Dahomey Basin.

Yenagoa, Bayelsa; some Niger Delta sites show very low EC and TDS, often $< 50\text{--}20 \mu\text{S}/\text{cm}$ and $< 20 \text{ mg/L}$, reflecting freshwater environment. It is observed in Lagos, Saudi Arabia exhibit EC ranging from 1000 to 1200 $\mu\text{S}/\text{cm}$ while TDS reveal up to 700 mg/L . This indicates they are moderately mineralised aquifers, reflecting dissolution and anthropogenic inputs. The coastal environment of Tanzania, specifically Kilwa Kisiwani exhibit very highly Saline and Mineralised Groundwater, indicating the water has very high EC (up to about 4600 $\mu\text{S}/\text{cm}$) with TDS ($>2500 \text{ mg/L}$), commonly due to coastal or evaporitic influences (Tables 12 and 13).

Table 12: The review of various corrosion and encrustation parameters their possible outcomes and implications

Table 13: Global perspectives of physicochemical parameters with data from the study area

6. Conclusion

This study provides comprehensive evidence that groundwater in the Eastern Dahomey Basin presents dual threats of corrosion and encrustation, with significant spatial variability correlated with coastal proximity and land use patterns. The hydrochemical analysis reveals that seawater intrusion, mineral dissolution, and anthropogenic activities collectively influence corrosion and encrustation processes. The application of multiple indices provides a robust assessment of these threats and offers insights for sustainable water resource management in coastal regions. The findings indicate that infrastructure development in the region must account for these hydrochemical challenges to ensure long-term sustainability and water security. The integration of geospatial analysis with hydrochemical assessment provides a valuable approach for targeted management interventions.

Based on the findings from the study area, it is recommended that the use of corrosion-resistant materials such as 316L stainless steel or high-density polyethylene (HDPE) for casing and pipelines in high-corrosion zones identified through spatial mapping. This can be complemented with introducing cathodic protection systems for existing mild steel infrastructure. Adopting periodic (6-month interval) descaling with citric acid for affected boreholes, coupled with calcite contactors installation to raise pH and LSI values in corrosive waters in order to reduce corrosion potential while maintaining water quality. Other recommendations include, establishing quarterly monitoring of LSI, RSI, and chloride concentrations in high-risk areas. Conduct annual video inspection of well casings to assess corrosion and encrustation damage. Enforce setback distances of at least 500 meters for new boreholes near the coastline to minimize seawater intrusion impacts. Develop integrated coastal zone management plans that address groundwater extraction

rates and land use practices affecting aquifer vulnerability. It is also proposed to conduct a long-term monitoring program to assess seasonal variations in corrosion and encrustation potentials. Investigating the effectiveness of various mitigation measures under local conditions will assist to combat the manance of corrosion-encrustation challenges. Above all, it is required to explore the potential of novel materials and coatings for improved corrosion resistance.

Acknowledgements

This research was supported by the Department of Mineral and Petroleum Resources Engineering Technology, The Federal Polytechnic, Ado Ekiti. The authors acknowledge the technical support provided by the Keys Laboratory of Cenozoic Geology and Environment, Institute of Geology and Geophysics, CAS, China. We also thank community members and local authorities for their assistance during field sampling.

Author's disclaimer

Funding

No specific funding was received for this study.

Informed Consent

Not applicable.

Ethical Approval

Not applicable.

Conflict of Interest

The author declares no conflict of interest.

Data Availability

All data generated or analyzed during this study are included in this published article.

Authorship credits

Author	A	B	C	D	E	F
ROF						

A - Study design/ Conceptualization B - Investigation/ Data acquisition
 C - Data Interpretation/ Validation D - Writing
 E - Review/Editing F - Supervision/Project administration

References

Abd-Elaty, I., et al. (2022). Controlling seawater intrusion in unconfined coastal aquifers through aquifer storage and recovery. *Journal of Hydrology*, 612, 128-145.

Abd-Elaty, I., et al. (2022). Cost-effective management measures for coastal aquifers affected by saltwater intrusion and climate change. **Science of the Total Environment**, 836, 155-174.

Aladejana JA, Kalin RM, Sentenac P, Hassan I. (2021. Groundwater Quality Index and Saltwater Intrusion in the Eastern Dahomey Basin, Nigeria. *Environ Earth Sci*;80:1–15.

Aladejana, J.A.; Kalin, R.M.; Sentenac, P.; Hassan, I. 2020. Groundwater Quality Index as a Hydrochemical Tool for Monitoring Saltwater Intrusion into Coastal Freshwater Aquifer of Eastern Dahomey Basin, Southwestern Nigeria. *Groundw Sustain. Dev.*, 25, 1–15.

Amah, E.A, Esu E.O. and Ntekum E.E.U. 2008. Evaluation of corrosion encrustation potential of groundwater wells in Calabar. *Global Journal of Geological Sciences*, 6(1), 1-7.

Appelo, C.A.J. & Postma, D. 2005. *Geochemistry, Groundwater and Pollution* (2nd ed.). CRC Press. <https://doi.org/10.1201/9781439833544>

Barlow, P.M. 2003. *Ground Water in Freshwater-Saltwater Environments of the Atlantic Coast*. USGS Circular 1262.

Etu-Efeotor, J.O, 1997. *Fundamentals of Petroleum Geology*. Published by Paragraphics (an imprint of Jeson services) .Port Harcourt. Pp.62, 64, 146.

Fakolade, O.R., & Obasi, R.A. (2012). The geochemical assessment of subsurface coastal plain clastic deposits of Eastern Dahomey Basin around Lagos area, South West Nigeria. *International Journal of Science and Technology*, 1(11) 300–307. [LinkResearchGate+2SCIRP+2SCIRP+2](https://doi.org/10.1201/9781439833544)

Garg, S.K. 2005. *Hydrology and Water Resources Engineering*. Khanna Publishers.

General Air Products. (2025). Understanding the 2025 Updates to NFPA 13: Key Changes for Vapor Corrosion Inhibitors.

Ikhanne, P. R., Ojo, A. O., & Ojo, O. J. (2018). Geochemical and mineralogical evaluation of the Maastrichtian sandstone in the Dahomey Basin, southwestern Nigeria: Implications for provenance and tectonic setting. *Journal of African Earth Sciences*, 145 1–14. DOI: [10.1016/j.jafrearsci.2018.05.005](https://doi.org/10.1016/j.jafrearsci.2018.05.005)

Johnson, E.E. 1975. *Groundwater and Wells*. UOP Inc.

Johnson, T.D., & Oluwajana, O.A. (2024). Elemental geochemistry of Cretaceous deposits in the Dahomey Basin (Nigeria): Implications for paleoclimatic and paleoenvironmental reconstructions. **Journal of African Earth Sciences**, 198, 104-122.

Larson & Skold 1958 Corrosion and tuberculation of cast iron, fourth report. Urbana, IL : reprinted from and copyrighted as a part of journal american water works association vol. 50, no. 11, november, 1958

Madukwe, H. Y., Obasi, R. A., Fakolade, O. R. & Bassey, C. E. (2015). Provenance, tectonic settings and source area weathering of the coastal plain sediments south west Nigeria. *Scientific research journal (SCIRJ)* 3(2) 2201-2796.

Mohammed S. Hussain, Hany F. Abd-Elhamid, Akbar A. Javadi, and Mohsen M. Sherif (2025). Management and Seawater Intrusion in Coastal Aquifer. *MDPI, Water* 2019, 11: 1 – 20, 2467; doi:10.3390/w1112246

Nsabimana, A., & Li, P. (2023). Hydrogeochemical characterization and appraisal of groundwater quality for industrial purpose using a novel industrial water quality index (IndWQI) in the Guanzhong Basin, China. *Geochemistry*, 83(1), 125922.

Offodile, M.E. 2002. *Groundwater Study and Development in Nigeria* (2nd ed.). Mecon Press.

Olofinlade, W.S., et al. (2018). *Modeling Earth Systems and Environment*, 4, 1405–1421.

Omaka Omaka, Frank IkennaNwabue, E. J. Itumoh David Igwe 2014. Physicochemical Parameters And Nutrients Variations Of Streams And Rivers In Abakaliki, Ebonyi State, Nigeria, *Global Nest Journal* 16(1):114-123

Oyeyemi, Kehinde D., Aizebeokhai, A. P., Olaajo, A. A., and Okon, Emmanuel (2023). Hydrogeophysical Investigation in Parts of the Eastern Dahomey Basin, Southwestern Nigeria: Implications for Sustainable Groundwater Resources Development and Management. *Water*, Volume 15, Issue 16, Article 2862. DOI: 10.3390/w15162862.

PMC. (2025). Coastal aquifers key contributors to ocean chemistry. *PMC National Center for Biotechnology Information*.

Reeve, R.W. and Uhlig, H. H. 2008. Corrosion and Corrosion Control. 2nd Edition, John Wiley & Sons Inc., Hoboken, 513. DOI:10.1002/9780470277270

Roberge, P.R. 2007. Corrosion Inspection and Monitoring (Vol. 2). John Wiley & Sons, Hoboken, NJ.

Sanigdha Acharya, S.K. Sharma &Vinita Khandegar (2019). Assessment and hydro-geochemical characterization for groundwater quality and corrosion-scaling potential. Data in Brief, 18, 928-938. DOI: [10.1016/j.dib.2018.03.120](https://doi.org/10.1016/j.dib.2018.03.120)

WHO (2017). Guidelines for Drinking-water Quality (4th ed.). World Health Organization.

Winston, R.B., 2020. GW_Chart version 1.30 : U.S. Geological Survey Software Release, 26 June 2020, <https://doi.org/10.5066/P9Y29U1H>

World Health Organisation WHO 2006. Guidelines for Drinking-Water Quality.

Accepted manuscript - uncorrected pre-proof.

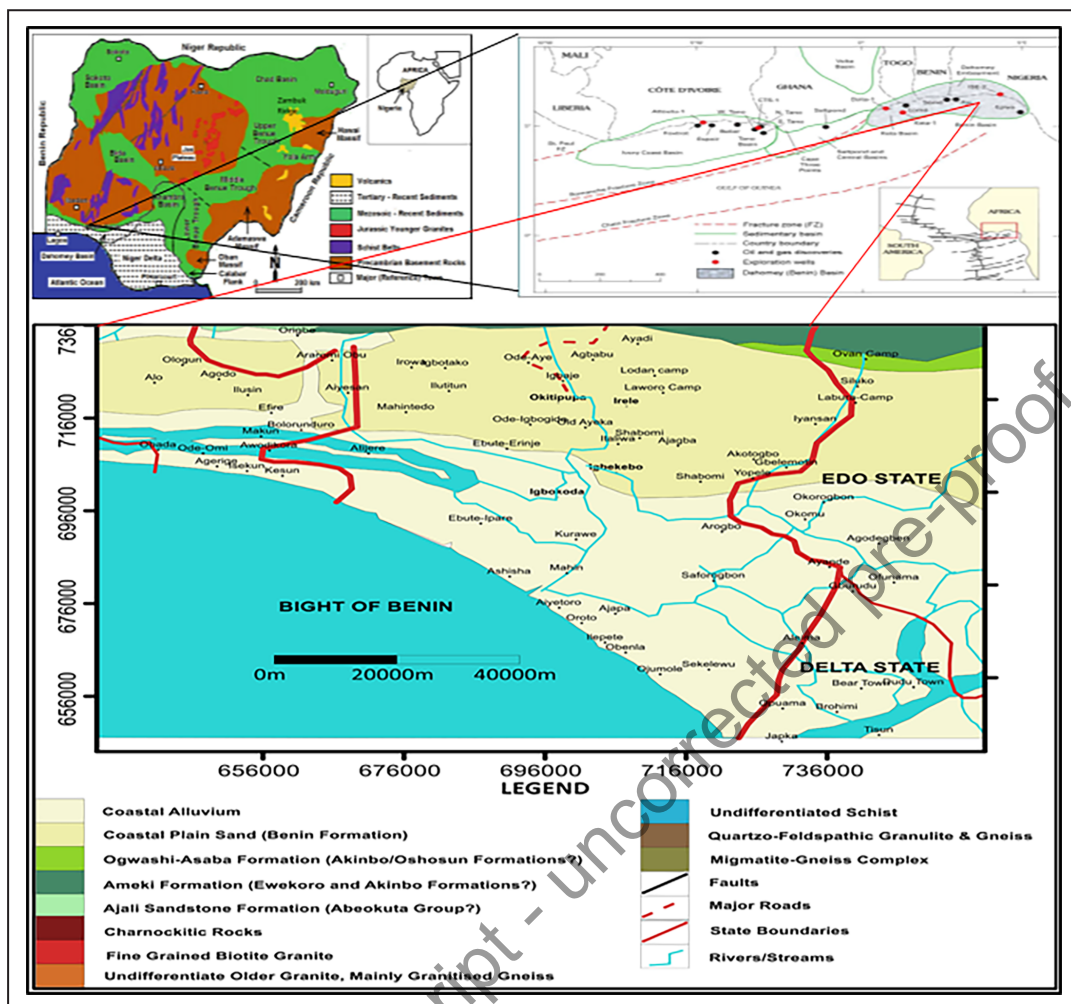


Figure 1: Map of the study area showing sample locations and geological features (retrieved from google 2025).

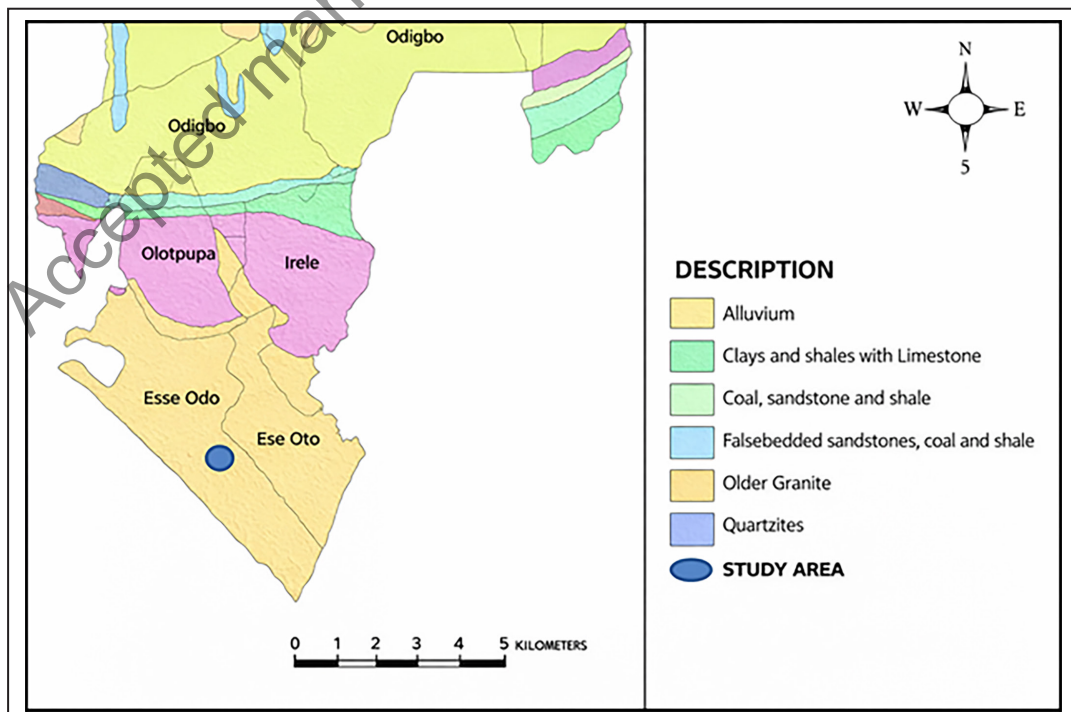


Figure 2: Geological map of the study area (Olabode & Mohammed, 2016)

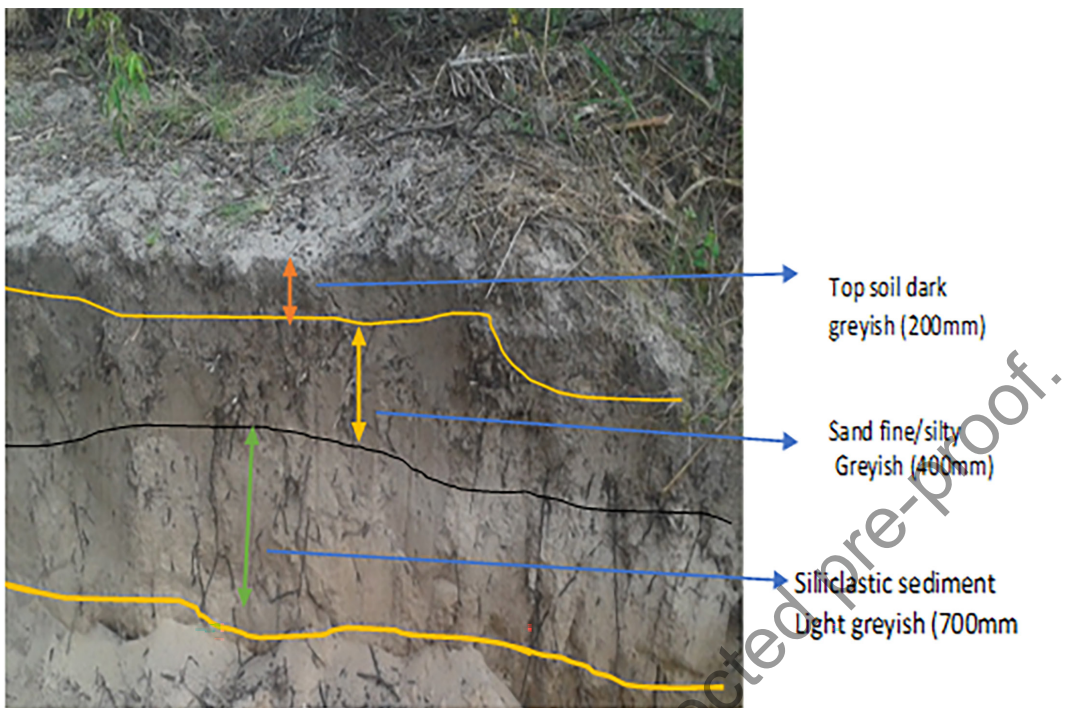


Figure 3: Photographs of outcrops from the study area showing sedimentary sequences

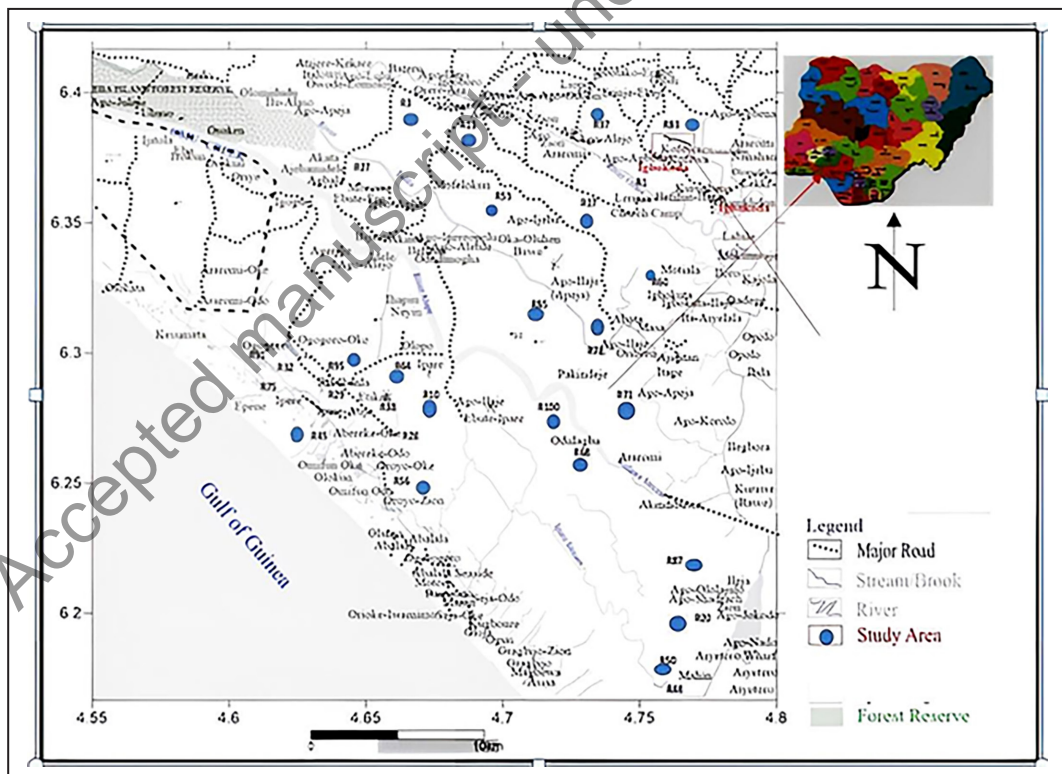


Figure 4: Map of the study area showing sampling point locations

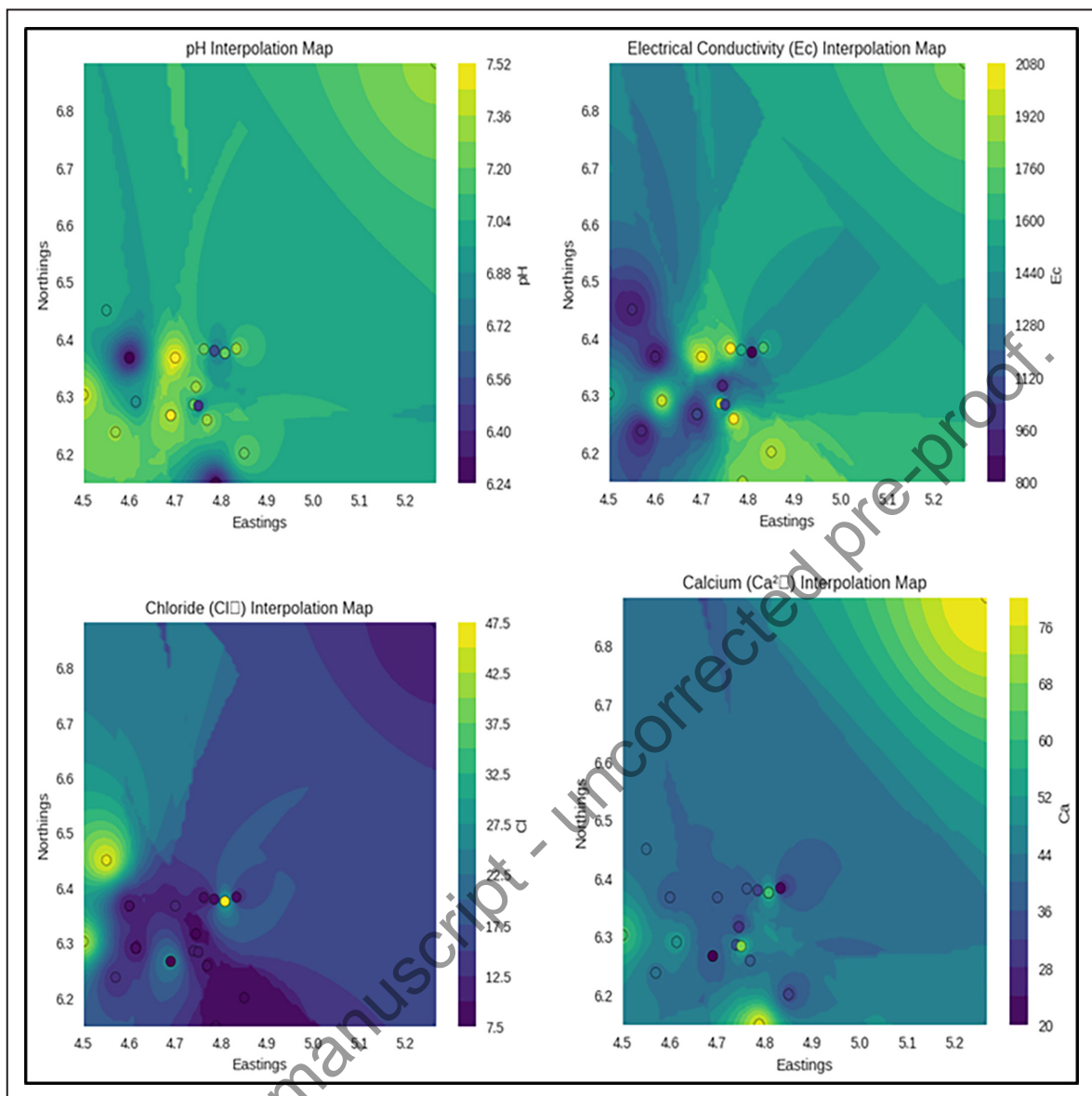


Figure 5a-d: Spatial distribution based in IDW Interpolation of (a) pH (b) electrical conductivity/TDS physicochemical parameters, and ion concentrations maps including (c) Chloride (d) Calcium across the study area

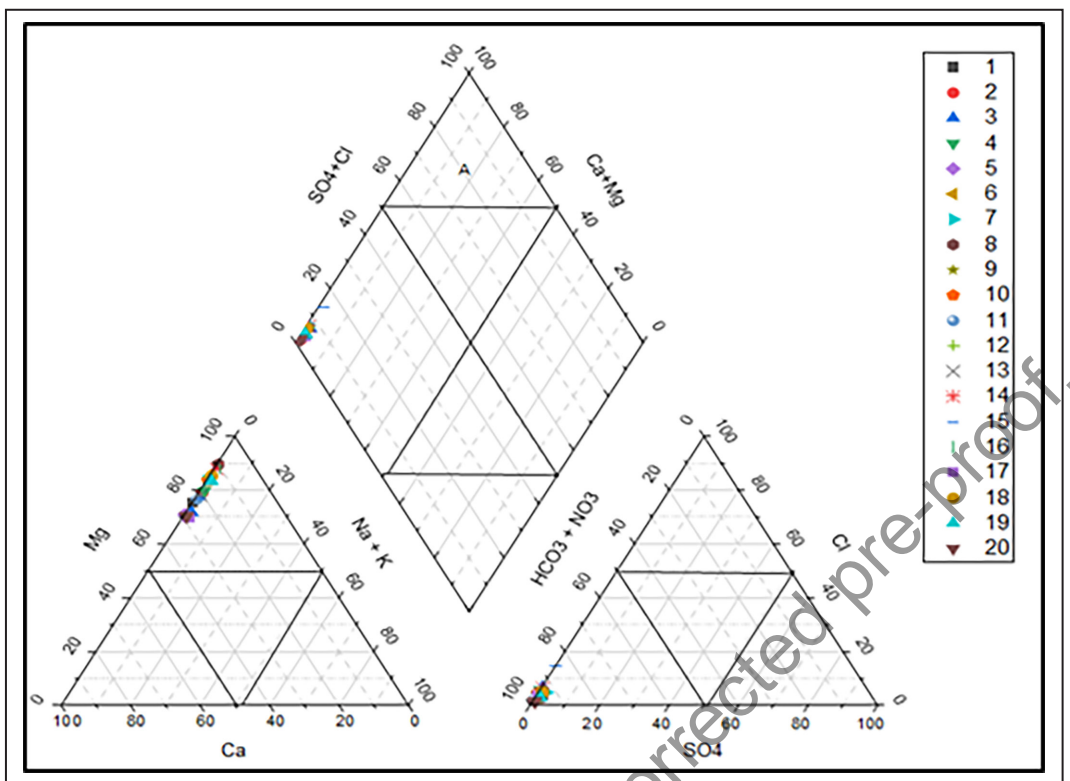


Figure 6: Piper diagram plotted using the Piper, template indicating hydrochemical facies of the samples under study

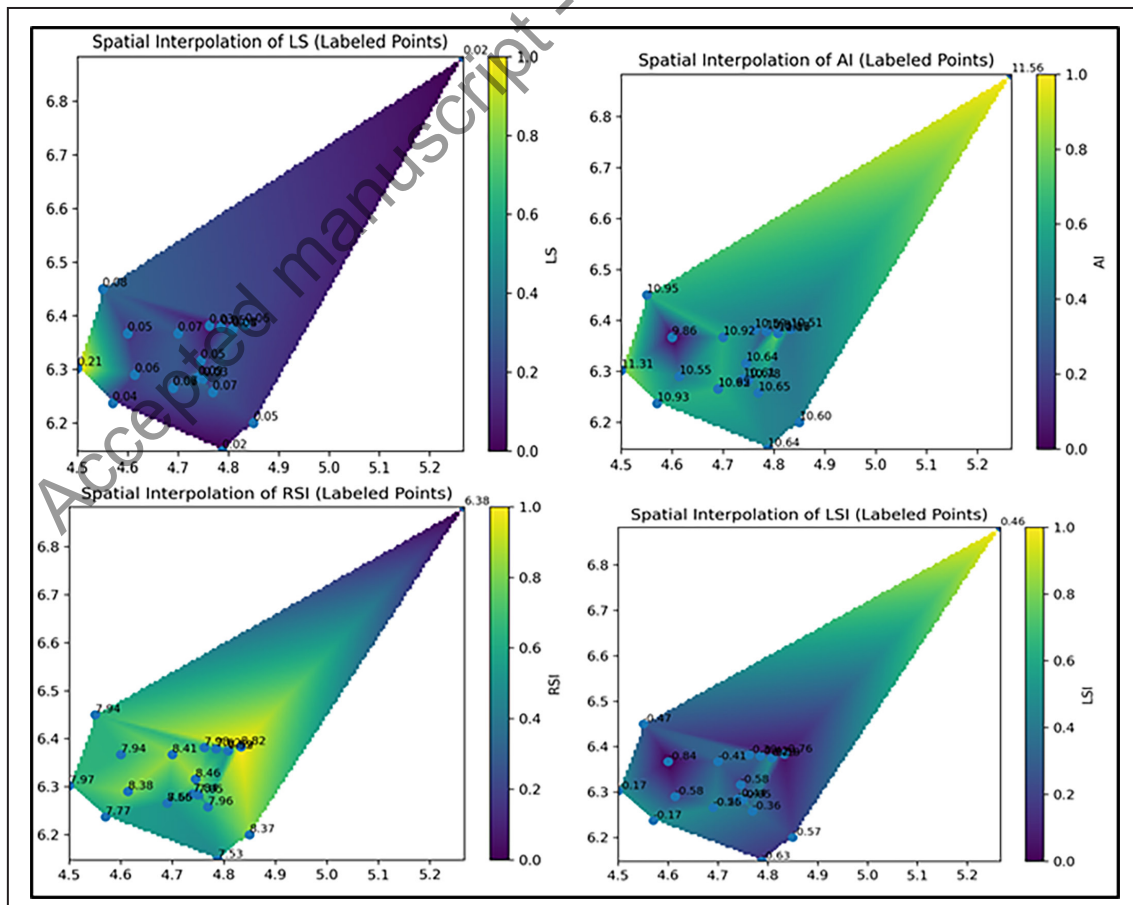


Figure 7a - d: Spatial distribution of Langelier Saturation Index (LSI), Aggressive index, Ryznar Stability Index (RSI) and Larson-Skold Index values across the study area

Table 1: Generalized stratigraphic column showing age, lithology, and aquifer characteristics in the eastern Dahomey Basin.

Age	Formation	Lithology	Thickness (m)	Aquifer Characteristics
Quaternary	Coastal Alluvium	Sand, clay, silt	0-50	Unconfined, high permeability
Tertiary	Benin Formation	Coastal Plain Sands	50-2000	Major aquifer system, high yield
	Jilaro Formation	Sandstone, clay	100-300	Confined aquifer
	Oshosun Formation	Clay, shale	50-200	Aquitard
	Akinbo Formation	Sand, clay	50-150	Semi-confined aquifer
Cretaceous	Ewekoro Formation	Limestone	10-30	Fractured aquifer
	Araromi Formation	Shale, sandstone	200-500	Confined aquifer
	Afowo Formation	Sandstone, siltstone	300-800	Minor aquifer
	Ise Formation	Sandstone, clay	200-600	Poor aquifer

Table 2: Corrosion -Encrustation Indices equations and their interpretations.

S/N	Index	Equation	Interpretation
1	Langelier (LS)	$LI = pH - pH_s$	$LI > 0$: Scaling; $LI < 0$: Corrosive
2	Ryznar (RSI)	$RI = 2pH_s - pH$	$RI > 6$: Corrosive; $RI < 6$: Scaling
4	Larson-Skold (LS)	$LS = (Cl^- + SO_4^{2-}) / (HCO_3^- + CO_3^{2-})$	$LS > 1.2$: High corrosion
5	Aggressive Index (AI)	$AI = pH + \log_{10}$	$AI < 10$: Very aggressive

Legend: Where: $pH_s = (9.3+A+B) - (C+D)$; $A = (\log_{10} (TDS) - 1) / 10$; $B = -13.12 * \log_{10} (C+273) + 34.55$; $C = \log_{10} (Ca^{2+} as CaCO_3) - 0.4$; $D = \log_{10} (alkalinity as CaCO_3)$; $pH_{eq} = 1.465 + \log_{10} (alkalinity) + 4.54$; H in AI index has Calcium hardness (mg/l)

Table 3: Classification criteria for corrosion and encrustation indices.

S/N	Index	Corrosive Tendency	Neutral	Scaling Tendency
1	LSI	< 0	0	> 0
2	RSI	> 6	6-7	< 6
3	LS	> 1.2	0.8-1.2	< 0.8
4	AI	< 10	10-12	> 12

Table 4: Results of Physicochemical analysis from the study area.

LOC	Eastings	Northings	Temp	pH	Ec	TDS	Salinity	Turbidity	HCO3	CO3
T1	4.808	6.375	30	6.5	1476	781	0.2	20.5	400	0.01
T2	5.267	6.883	29	7.3	1775	939	0.9	2.1	500	0.03
T3	4.808	6.375	25	7.2	714	378	0.2	4.6	600	0.01
T4	4.69	6.266	27	7.2	879	465	0.1	7.8	620	0.02
T5	4.785	6.379	29	6.6	1518	803	0.2	5.7	200	0.02
T6	4.769	6.258	30	7.3	2037	1078	1.3	15.2	180	0.01
T7	4.74	6.285	29	7.2	1887	993	1.2	1.5	180	0
T8	4.69	6.266	26	7.5	990	524	0.1	0.02	200	0.01
T9	4.57	6.237	25	7.3	860	455	0.1	1.2	460	0.06
T10	4.6	6.367	26	6.3	836	432	0.6	0.6	180	0.02
T11	4.75	6.283	27	6.5	990	771	0.5	5.5	420	0.01
T12	4.762	6.382	29	7.2	2035	969	0.1	14.4	380	0.03
T13	4.614	6.29	27	6.9	1899	377	0.03	1.6	160	0.02
T14	4.55	6.45	25	7.0	870	565	0.1	1.4	600	0.01
T15	4.5	6.302	28	7.4	1518	814	0.1	1.3	200	0.01
T16	4.833	6.383	27	7.3	1637	975	1.3	15.2	180	0
T17	4.85	6.2	29	7.2	1887	993	1.2	1.5	180	0.01
T18	4.7	6.367	28	7.5	1990	524	0.1	0.02	200	0.02
T19	4.745	6.316	26	7.3	860	455	0.1	1.2	220	0.02
T20	4.788	6.148	28	6.3	1836	432	0.6	0.6	600	0.01
Min			25	6.3	714	378	0.03	0.02	160	0
Max			30	7.5	2037	1078	0.9	20.5	620	0.06
mean			27.5	7.0	1424.7	684.8	0.4	5.097	333	0.017
WHO (2017)			6.5 -7.5		1500	1000	-	0.5NTU	-	

Table 5: Statistical summary of physicochemical parameters of groundwater samples in relation to WHO (2017) Standards.

S/N	Parameter	Minimum	Maximum	Mean	WHO (2017) Standard
1	pH	6.3	7.5	7.0	6.5-8.5
2	EC (μ S/cm)	714	2037	1424.7	1500
3	TDS (mg/L)	378	1078	684.8	1000
4	Temp (°C)	25	30	27.5	-
5	Salinity (PSU)	0.03	0.9	0.4	-

Table 6: Results of Ion Concentrations analysis of the samples under study.

LOC	Eastings	Northings	Cl	SO4	NO3	PO4	Na	K	Ca	Mg	Fe
T1	4.808	6.375	16	0.9	8.3	117.7	0.2	0.1	55.5	171.3	0.7
T2	5.267	6.883	10.6	0.7	0.3	45.1	2.1	2.1	79.9	318.1	0.6
T3	4.808	6.375	47.9	0.7	10	3.6	2.3	1.6	61.4	165.5	0.4
T4	4.69	6.266	40.8	1.5	6.1	4.9	2.4	1.2	50.5	212.7	0.5
T5	4.785	6.379	8.9	0.9	10.1	2.3	0.1	0	33.6	82.1	0.3
T6	4.769	6.258	8.9	2.8	14.9	15.6	0.7	0.1	38.7	219.8	0.8
T7	4.74	6.285	10.6	4.9	11.1	0.01	0.7	0.08	37	188.8	0.3
T8	4.69	6.266	7.1	4.5	12.3	5	0.8	0.01	21	187.9	0.8
T9	4.57	6.237	12.4	4.4	1	12.3	1.2	0.7	42.9	236.8	0.4
T10	4.6	6.367	8.9	0.02	0.2	1	1.3	0.01	37	193.3	0.3
T11	4.75	6.283	10.1	0.6	5.9	15.6	0.3	2.1	68.1	232.8	0.7
T12	4.762	6.382	8.8	1.3	11	1	1.7	0.1	37	212	0.8
T13	4.614	6.29	8.7	0.9	6.7	5	2.1	0.2	50.5	187.6	0.6
T14	4.55	6.45	45.8	2.8	10	2.3	1.3	1.4	41.4	317.9	0.5
T15	4.5	6.302	41.9	0.7	6.1	14.2	2.4	2.3	61.4	217.6	0.4
T16	4.833	6.383	8.7	1.5	10.1	0.01	2.2	1.6	22	182.3	0.8
T17	4.85	6.2	7.9	0.8	14.4	10.2	0.7	1.2	33.6	81.9	0.3
T18	4.7	6.367	11.6	2.7	11	12.3	1.7	0	36.7	222.1	0.9
T19	4.745	6.316	7.7	3.2	10	2.3	0.8	1.8	30.2	165.2	0.4
T20	4.788	6.148	8.7	4.3	0.6	4.9	2.4	0.1	76.7	187	0.3
Min			7.1	0.02	0.2	0.01	0.1	0.01	21	81.9	0.3
Max			47.9	4.9	14.9	45.1	2.4	2.3	79.9	318.1	0.9
mean			16.6	2.006	8.005	13.77	1.37	0.835	45.76	199.1	0.54
WHO (2017)			250	250	50		200		100	50	0.3

Table 7: Statistical summary of Ion Concentrations analysis of the samples under study relative to the WHO (2017) standards.

S/N	Parameter	Minimum	Maximum	Mean	WHO (2017) Standard
1	C ⁻	7.1	47.9	17.2	250
2	SO ₄ ²⁻	2.1	4.9	3.5	250
3	NO ₃ ⁻	0.02	12.3	7.4	50
4	Na ⁺	0.1	24	1.2	200
5	Ca ²⁺	21.0	79.9	45.8	100
6	Mg ²⁺	82.1	318.1	197.6	50
6	Fe	0.3	0.8	0.5	0.3

Table 8: Stability Indices Results per Sample from the study area.

LOC	Langlier Saturation Index (LSI)		Ryznar Stability Index (RSI)		Aggressiveness Index (AI)		Larson-Skold Index (LS)	
T1	0.29	Scaling	6.92	Mod. Scaling	10.87	Mod. Aggressive	0.04	Low Corrosion Pot.
T2	0.46	Scaling	6.38	Scaling	11.56	Mod. Aggressive	0.02	Low Corrosion Pot.
T3	-0.19	Corrosive	7.59	Corrosive	11.16	Mod Aggressive	0.08	Low Corrosion Pot.
T4	-0.25	Corrosive	7.65	Corrosive	10.95	Mod Aggressive	0.07	Low Corrosion Pot.
T5	-0.42	Corrosive	7.62	Corrosive	10.31	Aggressive	0.05	Low Corrosion Pot.
T6	-0.36	Corrosive	7.96	Corrosive	10.65	Aggressive	0.07	Low Corrosion Pot.
T7	-0.44	Corrosive	7.84	Corrosive	10.61	Aggressive	0.09	Low Corrosion Pot.
T8	-0.56	Corrosive	8.56	Highly Corrosive	10.62	Aggressive)	0.06	Low Corrosion Pot.
T9	-0.17	Corrosive	7.77	Corrosive	10.93	Mod. Aggressive	0.04	Low Corrosion Pot.
T10	-0.84	Corrosive	7.94	Corrosive	9.86	Very Aggressive	0.05	Low Corrosion Pot.
T11	-0.05	Corrosive	7.05	Mod. Scaling	10.78	Mod Aggressive	0.03	Low Corrosion Pot.
T12	-0.39	Corrosive	7.98	Corrosive	10.59	Aggressive	0.03	Low Corrosion Pot.
T13	-0.58	Corrosive	8.38	Highly Corrosive	10.55	Aggressive	0.06	Low Corrosion Pot.
T14	-0.47	Corrosive	7.94	Corrosive	10.95	Mod. Aggressive	0.08	Low Corrosion Pot.
T15	-0.17	Corrosive	7.97	Corrosive	11.31	Mod. Aggressive	0.21	Mod. Corrosion Pot.
T16	-0.76	Corrosive	8.82	Highly Corrosive	10.51	Aggressive	0.06	Low Corrosion Pot.
T17	-0.57	Corrosive	8.37	Highly Corrosive	10.60	Aggressive	0.05	Low Corrosion Pot.
T18	-0.41	Corrosive	8.41	Highly Corrosive	10.92	Mod. Aggressive	0.07	Low Corrosion Pot.
T19	-0.58	Corrosive	8.46	Highly Corrosive	10.64	Aggressive	0.05	Low Corrosion Pot.
T20	-0.63	Corrosive	7.53	Corrosive	10.64	Aggressive	0.02	Low Corrosion Pot.
Min	-0.84		7.05		9.86		0.086	
Max	0.46		8.82		11.56		0.026	
Mean			6.9		8.056		0.060	
Corr	90%		30%		100%		0%	
Enc	10%		70%		0%		100%	

Table 9: Summary of Corrosion and Encrustation indices for groundwater samples under study.

S/N	Index	Range	Corrosive (%)	Neutral (%)	Scaling (%)	Classification Criteria
1	LSI	0.6 to 1.2	41	0	59	LI < 0: corrosive LI > 0: scaling
2	RSI	6.8 to 9.2	88	0	12	RSI > 6: corrosive RSI < 6: scaling
3	AI	6.3 to 9.3	41	0	59	AI < 10: corrosive AI > 12: scaling
4	LS	0.05 to 1.8	38	0	62	LS > 1.2: corrosive LS < 0.8: scaling

Table 10: Description of corrosion and encrustation indices compared with various standards.

Parameters	Result (CEIP)	Mean	Johnson 1975	WHO 2006	Remark
pH	6.3 – 7.5	7.0	Corrosive pH<7 Encrustation pH>7	Acidic Ph<7 Alkaline Ph>7	Encrustation
Temperature °C	25 – 30	27.5	Corrosive temp >27C	-	Corrosive
TDS (mg/l)	378 – 1078	684.8	Corrosive TDS>1000 mg/l	<1000	Encrustation
EC (µS/cm)	816 – 2037	1294.2	Corrosive EC>1500 µS/cm	-	Encrustation
Fe (mg/l)	0.3 – 0.9	0.5	Encrusting Fe>0.3	<0.3	Encrustation
Mn (mg/l)	ND	ND	Encrusting Mn>0.1	<0.05	ND
DO (mg/l)	ND	ND	Corrosive DO>2.0	-	ND
H ₂ S (mg/l)	ND	ND	Corrosive H ₂ S>2.0	-	ND
Cl ⁻ (mg/l)	7.1 – 47.9	17.2	Corrosive Cl>500	200	Encrustation
HCO ₃ ⁻ (mg/l)	ND	358	Corrosive HCO ₃ >50	-	ND
Total Hardness (mg/l)	22.0 – 226.4	76.9	Encrusting THC>100	100	Corrosive

Table 11: Descriptive summary of corrosion and encrustation indices reference to specific sample locations.

Zone	Parameter signals	Likely issue
Around T6, T12, T16-T18	High TDS + moderate salinity	Corrosion risk due to mineralised water; possible scale where Ca/Mg high
T13	Very high salinity (≈3‰), moderate TDS	Severe corrosion potential; brine may attack metal/cement
Sites with >400 mg/L HCO ₃ ⁻ & pH ~7	Bicarbonate + hardness likely	Scaling/encrustation risk (CaCO ₃ precipitation)

Table 12: The review of various corrosion and encrustation parameters their possible outcomes and implications.

Location	Parameters Measurement	Results	Implications
Dahomey: Benin coastal aquifer	Extent of seawater intrusion; hydrochemical facies; delineation of boundary zones of intrusion.	Areas like Dahomey show evidence of seawater intrusion; certain wells are contaminated. Salinity, chloride elevated beyond background.	Even moderate saline intrusion several km inland; demands monitoring & management.
Parts of Niger Delta, Nigeria	Saltwater intrusion in coastal island aquifers; depth to interface; hydrochemical ratios.	Depth to freshwater-saltwater interface as shallow as 10–15 m , depending on tidal phase/elevation. Strong hydrochemical signals: elevated TDS, EC, salinity, Cl ⁻ , Na ⁺ , K ⁺ .	Very shallow interface means wells are highly vulnerable; infrastructure in shallow wells likely exposed to corrosive/inhospitable water.
Eastern Saudi Arabia (multi-layered aquifers)	Effects of seawater intrusion on groundwater quality; suitability for human/agricultural use.	Documented elevated salinity, poor suitability in some zones; groundwater becomes "unsuitable" for some uses as intrusion increases. Exact thresholds vary, but values well exceeding safe drinking/irrigation limits in affected layers.	Coastal aquifers under strong stress from human use + hydrochemical shift; management and/or mitigation required.
Global / General Coastal Context	Rates / extent of intrusion; risk behavior; role of over-pumping and sea level rise.	>1% seawater mixing makes water non-potable by taste; sea level rise of ~10cm can move interface inland hundreds of meters (on shallow gradients) in some coastal plains. In Spain: ~58% of the 82 coastal hydrogeological units show some seawater intrusion.	Coastal aquifers worldwide are already impacted; even small degrees of intrusion shift hydrochemistry enough to affect usability, corrosion, etc.

Table 13: Global perspectives of physicochemical parameters with data from the study area.

Location	EC Range ($\mu\text{S}/\text{cm}$)	TDS mg/L	Salinity (PSU)	pH	(Cl ⁻) mg/L
Study Area	1424.7	684.8	0.4	7.0	16.6
Niger Delta	19–24	9–183	0.17		
Bayelsa	6.23–13.74	5.77–18.30			
Lagos	450–1190	247.5–589.7			
Saudi Arabia	382–1214	258–775		6.65–8.26	19–202
Gombe	193.9–350	198–345			
Tanzania	1160–4620	754–3003			